Dynamic distribution of Spatial during mouse spermatogenesis and its interaction with the kinesin KIF17b

Murielle Saade[a], Magali Irla[a], Jérôme Govin[b], Genevieve Victorero[a], Michel Samson[c], and Catherine Nguyen [a,*]

[a] INSERM, ERM 206, Case 928, Parc Scientifique de Luminy, 13288 Marseille Cedex 9, France ; Université Aix-Marseille II, Marseille, France.

[b] INSERM, U309, Laboratoire de Biologie Moléculaire et Cellulaire de la Différenciation, Institut Albert Bonniot, Faculté de Médecine, 38706 La Tronche Cedex, France

[c] INSERM, U620, Faculté de Médecine-Pharmacie, Université de Rennes I, 2 avenue du Prof. Léon Bernard, 35043 Rennes cedex, France ; Université de Rennes I, 2 avenue du Prof. Léon Bernard, 35043 Rennes cedex, France

* Corresponding author. Laboratoire TAGC INSERM ERM 206, Case 928, Parc Scientifique de Luminy, 13288 Marseille Cedex 9, France. Tel.: 33-4-91-82-75-02; Fax: 33-4-91-82-75-00.

E-mail adress: nguyen@tagc.univ-mrs.fr (C Nguyen).

Abstract

Spatial gene is expressed in highly polarized cell types, such as epithelial cells in the thymus, neurons in the brain and germ cells in the testis. In this study, we report the characterization and the distribution of Spatial proteins during mouse spermatogenesis. Besides Spatial-ε and -δ, we show that the newly described short isoform Spatial-β is expressed specifically in round spermatids. Using indirect immunofluorescence, we detected Spatial in the cytosol of early round spermatid. By the end stages of round spermatids, Spatial is concentrated at the opposite face of the acrosome near the nascent flagellum and in the manchette during the elongation process. Finally in mature sperm, Spatial persists in the principal piece of the tail. Moreover, we found that Spatial colocalizes with KIF17b, a testis-specific isoform of the brain kinesin motor KIF17. This colocalization is restricted to the manchette and the principal piece of the sperm tail. Further, coimmunoprecipitation experiments of native proteins from testis lysate confirmed Spatial-KIF17b association through Spatial-ε long isoform. Together, these findings imply a function of Spatial in spermatid differentiation as being a new cargo of the kinesin KIF17b in a microtubule-dependent mechanism specific to the manchette and the principal piece of the sperm tail.

Keywords: Spermatogenesis, Spatial, Morphogenesis, Manchette, Spermatozoa, Principal piece, Kinesin motor KIF17b.

Introduction

Spermatogenesis is a complex process resulting at the production of functional sperm in the testis. Three phases can be distinguished: (a) mitotic proliferation of spermatogonia that provides a pool of stem cells, (b) meiotic divisions of spermatocytes that generate haploid spermatids, and (c) spermiogenesis, a process of differentiation of spermatids ending with the release of viable sperm into the lumen of seminiferous tubules [1]. Spermiogenesis in mice is divided roughly into processes occurring in round spermatids (steps 1-8) and those occurring in elongating spermatids (steps 9-16) [1]. In round spermatids, the acrosome starts to differentiate [2]. In step 8, the manchette begins to form when the shape of the nucleus changes from spherical to slightly elongated [3]. In step 9, the nucleus becomes even more elongated, and the manchette runs parallel to the nuclear envelop [3]. At later steps, the mitochondria become arranged in a spiral around the base of the flagellum, a fibrous sheath is deposited around the flagellar axoneme, and the nuclei become elongate, dense and compact [4]. All of these processes of massive differentiation and rapid polarization require transport and specific localization of vesicles, proteins and organelles. A number of kinesin and dynein superfamily motor proteins were proposed to carry out these transport processes in a microtubule-dependant manner during mouse spermiogenesis [5].

Spatial (Stromal Protein Associated with Thymii and Lymph-node) gene was screened by our laboratory from an adult mouse thymus library of cDNA clones using array technology [6]. This study was performed between *wild-type* and several *knock-out* mice models displaying a stromal disorganization in order to clarify stromal molecular mechanisms involved in T cell development [6]. The sequencing of these cDNA clones showed that they correspond to two adult variants previously described in the thymus by flomerfelrt et al. (GenBank accession nos. **AF257502** and **AF257503**) [7]. In addition, by screening 15 days embryonic thymus mouse

library, another new Spatial cDNA clone was isolated (GenBank accession no. **AY243459**) [8]. We reported the expression of this third isoform containing an additional exon of 69 bases in the thymus (GenBank accession no. **AY243457**) [8]. According to the size of alternative spliced variants, the longest and the shortest isoforms were respectively named Spatial-α (1035 bp) and Spatial-γ (933 bp) and the third new mid-sized isoform, Spatial-β (1002 bp) [8]. In addition, we also described two other isoforms in the testis: Spatial-ε (1454 bp) for the longest (GenBank accession no. **AF521592**) and Spatial-δ (1353 bp) for the shortest (GenBank accession no. **AF521591**) [9].

Then, this gene generates at least these five alternative splice variants: three short isoforms (Spatial-α, -β and -γ) and two long isoforms (Spatial-δ and -ε) with a tissue-specific distribution [8]. These isoforms appear to have no significant structural or protein counterparts which could reflect some functional homologies conserved with well defined protein families. Extensive use of databases and protein prediction programs show that Spatial short isoforms conserve a nuclear localization sequence (NLS) and proline rich domains. However, long isoforms do not present NLS sequences and possess more alpha-helix with an additional rich leucine sequence in the C-terminal of the proteins [8]. In the testis, we previously showed that Spatial long isoforms are tightly regulated during male sexual maturation and that Spatial messengers are restricted to step 2–10 spermatids [9].

In order to find out the role of this gene, we report the distribution and regulation of Spatial protein expression throughout spermatogenesis. In addition to Spatial long isoforms, specific antibody raised against Spatial subunits reveals the expression of the newly described short isoform Spatial-β [8]. We followed the distribution of Spatial in isolated germ cells. During spermatid differentiation, we showed that Spatial is concentrated at the opposite phase of the

acrosome near the nascent flagellum and is associated with the manchette during the elongation process. In spermatozoa, we showed that Spatial is concentrated in the principal piece of the flagellum where it colocalizes with the kinesin motor KIF17b, the testis-specific isoform of the brain kinesin-2 motor protein KIF17 [10]. Spatial-KIF17b colocalization was also studied in another highly organized microtubular array, the manchette. The interaction between Spatial and KIF17b was shown by coimmunoprecipitation of native proteins from testis lysate. In light of these findings, we discuss the involvement of Spatial in morphogenesis process and its potentiality to be a new cargo of the kinesin motor KIF17b confined to the manchette and the principal piece of the sperm tail.

Materials and methods

Animals and antibodies

Eight weeks old mice C57BL/6 were maintained under specific-pathogen free conditions. All experimental and surgical procedures were approved by the veterinary office of the Ministry of Agriculture, France (autorization number:13-27). Testes from *act* $^{-/-}$ mice were kindly provided by Dr. Noora Kotaja and Dr. Paolo Sassone-Corsi. Spatial polyclonal antibody was produced by immunizing rabbits against the mouse recombinant 6xHis-Spatial-α protein and further purified on a protein G column (Eurogentec). For immunofluorescence, mouse polyclonal anti-α-tubulin and anti-GM130/Golgin95 antibodies (Ab) were kindly provided by Dr. Stéphane Meresse (CIML, Marseille, France) and the mouse polyclonal anti-β-tubulin Ab as the goat polyclonal M-20 anti-KIF17 Ab from Santa cruz biotechnology. Secondary Abs correspond to the Alexa 546–goat anti–rabbit IgG, Alexa 488-goat anti-mouse IgG and the Alexa 488-donky anti-goat IgG (1/1000; Molecular Probes).

Spermatogenic cell fractionation

Spermatogenic cells were fractionated using the Bellvé method [11]. Briefly, adult mice testis were dissected, and processed to obtain an homogenous cell suspension. Cells were laid on the top of a 2-4% BSA gradient in an airtight sedimentation chamber at 4°C. Cells sediment according to their size, density and fractions were collected after 70 min. Stages were identified using a phase-contrast microscope. Fractions were pooled to obtain cell populations enriched at 90 % in each major stages. The fraction composed of late spermatids is obtained by sonication [12]. Mouse testis was homogenized in M1 buffer (0.32 M sucrose, 1.5 mM $CaCl_2$, 10 mM Tris pH 8, 1 mM DTT and antiprotease cocktail Complete, Roche), in a motor driven potter. Suspension was filtered through cloth sheet. Cells were pelleted, resuspended in M1 buffer supplemented with 0.1% Triton X-100 (M2), and sonicated at 500 J. Two washes were performed, first with M2, then with M1+0.88 M sucrose to separate condensed spermatids from cell fragments. Each cell suspension was subjected to proteins and total RNA extractions.

Isolation of mouse germ cells and spermatozoa

Testes of adult mice were dissected, and the albuginea were removed. Seminiferous tubules were released by a 10-min incubation at 37°C in 10 ml of a collagenase solution (1 mg/ml in phosphate-buffered saline PBS, Sigma). Tubules were then allowed to sediment at the bottom of the tube. the collagenase solution was replaced by 2 ml of the sedimentation medium (Ham F-12 medium, GIBCO) containing 0.5% bovine serum albumin (BSA) and Dnase (2 µg/ml) (Sigma). Germinal cells were then released from the tubules by pipetting for approximately 10 min with a glass Pasteur pipette until a homogenous cell suspension was obtained, which was then filtered

twice using 100-µm-pore-size filters (Becton Dickinson) and centrifuged (134 g for 10 min at 4°C). The cell pellet was then washed again in PBS at 4°C (10 min at 134 g). For Spermatozoa isolation from testis, the seminiferous tubules were freed carefully with two pairs of tweezers and washed in 5 ml fresh Hanks' balanced salt solution (HBSS) three times (Invitrogen). Seminiferous tubules were mechanically teased and were allowed to stand for 10 min at 37 C. Spermatozoa from cauda epididymidis and vas deferens were obtained after mincing these tissue and dispersion in HBSS. Suspensions were also allowed to stand for 10 min at 37 °C. The cloudy upper layer of these suspensions were recovered and was passed through 100-µm-pore-size filters to remove the debris. The spermatozoa were pelleted by centrifugation at 500 g for 10 min. Germ cells and sperm pellets thus obtained were resuspended and mounted on poly-L-lysine slides (Sigma) and processed for immunofluorescence analysis. Quality of these preparations was controlled using a phase-contrast microscope.

Histological analysis

Germ cells collected from testis and Sperm collected from cauda epididymis and vas deferens were fixed with 4% paraformaldehyde, and washed in PBS. Slides were permeabilized with 0.2% Triton X-100 for 10 min, and nonspecific sites were blocked with 5% BSA for 1 h. For indirect immunofluorescence, Spatial (1:1000) and KIF17 (1:200) polyclonal antibodies as GM130/Golgin95 (1/200), α-tubulin and β-tubulin antibodies (1:1000) were applied for 1 h. Preimmune antisera were used at the same concentration as negative control. After rinsing, sections were incubated again with the blocking buffer (3% BSA, 0.01 % Triton X-100 in 0.1M Tris buffer pH 7.4) for 15 min, then with the secondary antibody. Nuclei were stained with the 4', 6'-diamidino-2-phenylindole (DAPI) at 1 µg/ml (Calbiochem). Sections were mounted with

Mowiol fluorescent mounting medium (Calbiochem). Fluorescent images were acquired by Zeiss LSM 510 confocal microscopy. For cryosections, testes were embedded in optimum cutting temperature (OCT) compound (Sakura Finetech) and frozen in dry ice. Six-micrometer-thick cryosections were mounted onto glass slide. Sections were fixed with ice-cold methanol for 20 min at –20°C and subjected to the same protocol of indirect immunofluorescence mentioned above. Immunohistochemistry analysis was performed using the Histomouse^{TM}-Max kit with an avidin-peroxidase conjugate system (Zymed laboratories). Endogenous peroxidase activity was quenched by incubating slides for 10 min in 1% hydrogen peroxide diluted in PBS and the antibody-enzyme complex was visualized with the AEC substrate-chromogen. Incubation times were carefully monitored to prevent saturation, thus favouring visualization of differences in expression levels. Sections were counterstained using the hematoxylin solution (Zymed laboratories) and cover slipped using GVA mounting solution (Zymed laboratories) for examination. Images were taken using Zeiss, axiophot 2 microscope with Nikon digital camera DXm1200.

Immunoprecipitation

To prepare resin immobilized antibodies, polyclonal Abs for Spatial and control IgG (20 µg) were diluted with coupling buffer (0.1 M $NaHCO_3$ buffer containing 0.5 M NaCl, pH 8.3) and were incubated with cyanogen-bromide activated resin for 4 h (Sigma). Unreacted ligand was washed away with the coupling buffer and resin unreacted groups were blocked with 0.2M glycine, pH 8.0 for 2 hours. Finally the resin was washed extensively to remove the blocking solution, first with basic coupling buffer, then with acetate buffer 0.1M, pH4 containing 0.5M NaCl. This wash cycle of high and low pH solution was completed 3 times. For

immunoprecipitation, mouse testis extract (1 mg) was incubated overnight with resin immobilized antibodies in a final volume of 1 ml of immunoprecipitation buffer (TBS, 0.1% Tween 20) in the presence of proteinase inhibitor mixture (Sigma). The resin were then collected by centrifugation at 6000 rpm for 30 sec. and washed four times with 1 ml of immunoprecipitate buffer. To recover precipitated proteins, the resin was resuspended overnight at 4°C in 20 µl of SDS gel loading buffer without β-mercaptoethanol to not disturb the antibody structure. After a brief spin down the supernatant was collected and boiled for 5 min with SDS gel loading buffer containing β-mercaptoethanol and proteins were separated by 10% SDS-polyacrylamide gel (Invitrogen). For immunoprecipitation with KIF17 antibody, the resin was replaced by 50 µl of protein A-agarose beads (Zymed Laboratories) and precipitated proteins were proceeded to the same wash with TBS, 0.1% Tween 20 and elution with SDS gel loading buffer containing β-mercaptoethanol as mentioned above.

Western blots

Soluble and non-soluble protein fractions were separated by using the Nuclear Protein Extraction Kit (Panomics). Protein concentrations were measured using the Pierce BCA protein assay. Samples were electrophoresed on SDS-polyacrylamide gel already prepared (Invitrogen) (10% acrylamide) and transferred to Nitrocellulose membranes (BioRad) following incubation with the purified Spatial polyclonal antibody (1:2500) or the anti-KIF17 antibody (1:500). The staining was visualized using horseradish peroxidase-conjugated secondary antibody (1:1000; Amersham Pharmacia Biotech) and the enhanced chemiluminescence (ECL) detection system (Pierce). Quantitative analysis of Spatial proteins expression was performed using ImageJ software (National Institute of Health, USA).

Quantitative TaqMan RT-PCR

Total RNA was purified using TRIzol reagent (Gibco-BRL, Life Technologies). Quantitative RT-PCR was performed using the ABI PRISM 7000 Sequence Detection System. Random hexamers and the TaqMan reverse transcription reagents from the RT reaction mix (Applied Biosystems) were used to reverse transcribe total RNA. After, the PCR step was performed with TaqMan universal PCR master mix and assays-on-demand gene expression probes (Applied Biosystems). Primers and the TaqMan probe used to detect specifically short isoforms were: forward primer: 5'- TTGGAACCAGCCCCTGTTT -3', reverse primer 5'- GTTCTCCGGCTTCGTCTCT-3' and FAM 5'- CCCAGCTTTCTACTTCTG -3' NFQ, respectively. Primers and the TaqMan probe used to detect specifically long isoforms were: forward primer: 5'-GCTTCAAGAGCCTCAAGAGACA-3', reverse primer 5'-GGTGGTGACCTAGTCTTCTTCAG-3' and FAM 5'-CCTTTGGACTAGTCACCTCAT -3' NFQ. The 18S-rRNA was amplified from all samples on each plate as a housekeeping gene to normalize expression between different samples and to monitor assay reproducibility. A non-template control was included for each target analyzed. Relative quantification of all targets was calculated by using the comparative cycle threshold method [13].

Results

Characterization of Spatial proteins in the mouse testis

Spatial polyclonal antibody was generated against the mouse recombinant 6xHis-Spatial-α protein that shares a conserved sequence with all other Spatial isoforms and further purified on a protein G column. To test the specificity of this antibody, we performed a Western blot analysis on non-soluble (ns) and soluble (s) fractions of purified round spermatids (RS) isolated from

adult mouse testis in which mRNAs of Spatial long isoforms are highly expressed (Fig. 1A) [9]. Spatial antibody reacts strongly with two proteins at 52 and 49 kDa in the soluble fraction, corresponding to Spatial-ε and Spatial-δ long isoforms, respectively. Moreover an additional band at 34 kDa that could correspond to the recently characterized isoform Spatial-β was also detected [8]. Bioinformatic analysis based on the cDNA sequences predicted a molecular mass of 43.8 kDa for Spatial-ε, 40.2 kDa for Spatial-δ and 24.6 kDa for Spatial-β [8]. The apparent mobility of the *in vivo* proteins could be explained by post-translational modification processes. In addition two minor bands were also detected which could be unspecific as they could correspond to other uncharacterized isoforms (Fig. 1A). In order to confirm that the protein at 34 kDa corresponds to the isoform Spatial-β, we performed quantitative TaqMan RT-PCR analysis with specific TaqMan probe and primers on mRNAs extracts of purified pachytene spermatocytes (PS), round spermatids and a pool of round and elongating spermatids (RES, Fig. 1B) [8]. Spatial short isoform mRNAs appears in pachytene spermatocytes with a higher expression in round spermatids partially diluted in the pool of round and elongating spermatids. Altogether, these results confirm the presence of the short isoform Spatial-β in the testis recognized by the affinity-purified Spatial-antibody in addition to the testis specific Spatial-ε and -δ long isoforms.

Quantification of Spatial isoform levels in isolated germ cells

To determine the expression profile of Spatial proteins during spermatogenesis, we performed Western blot analysis on isolated mouse testicular cell types that reflect the strictly controlled spermiogenesis program (Fig. 2). A very weak signal of Spatial-ε and -δ is detected in pachytene spermatocytes that represent the last meiosis cell type. This drastically increases in round

spermatids and become very strong in the round/elongating and elongated spermatids (ES, Fig. 2A). This expression further decreases in condensed spermatids (CS) to persist in spermatozoa (Spz). Since the expression profile of Spatial-δ and -ε is similar, Spatial-β is specifically expressed in round spermatids to further drastically reduce in spermatids under maturation. In addition, the expression profile of Spatial isoforms during spermatogenesis was quantified by optical density measurements (Fig. 2B). Results showed that Spatial long isoforms expression increases during the elongation process of round spermatids while Spatial-β expression is reduced 3-fold between round and round/elongating spermatids (Fig. 2B). The diminution of Spatial-β expression during later stages of mouse spermatogenesis could be related to the ACT/CREM transcriptional complex required for spermatid maturation [14, 15] since the expression of Spatial-β is significantly high in *act* null mice while Spatial long isoforms remain unchanged (Supplementary data). Altogether, these findings show that Spatial long isoforms expression correlates with stages associated with drastic morphological changes of germ cells [1] while Spatial-β is exclusively expressed in round spermatids.

Distribution of Spatial in specific seminiferous tubules during spermatogenesis

In order to determine the distribution of Spatial during spermatogenesis, we also used the purified Spatial polyclonal antibody to perform histological analysis on adult mouse testis sections (Fig. 3). Testis sections were subjected to immunofluorescence analysis of Spatial and counterstained with the DAPI marker to visualize the nuclear morphology (Fig. 3A-D, E-G, L-N). We observed a restricted expression of Spatial proteins in some of seminiferous tubules where spermiogenesis takes place (Fig. 3A-C). We detected abundant staining in round spermatids at stage VIII (Fig. 3A). A higher magnification at this stage showed that the localization of Spatial proteins in round

spermatids is exclusively cytosolic with an intense signal seen in structures or organelles near the nucleus of some round spermatids (Fig. 3E, arrowheads). Spatial staining is maintained in elongating spermatids at stages IX-X (Fig. 3B). A higher magnification at these stages showed a staining in ring-like structures in elongating spermatids (Fig. 3F, G, arrowheads). The ring-like Spatial signals colocalize with or are adjacent with β-tubulin-positive structures indicating that Spatial associates with the manchette, a highly organized microtubule structure involved in the nuclear shaping of round spermatids (Fig. 3L-N). At the end of elongation stages, a bright fluorescence is detected within tubule lumens suggesting a localization of Spatial in the forming tail (Fig. 3C). In similar sections exposed to the preimmune serum instead of primary antibody, little or no fluorescence was observed over any portions of seminiferous tubules (Fig. 3D). In addition, we also analysed mouse testis sections by immunohistochemistry (Fig. 3H-K). As shown, Spatial proteins were highly expressed in round spermatids at stage VIII and present a slender staining at stages IX-X that appears to be associated with the manchette, which is consistent with the result obtained by confocal microscopy (Fig. 3H, I, inset). At higher magnification, we also observed the cytosolic distribution of Spatial at stages VII-VIII while at later stages of round spermatids (VIII- IX), an intense signal is localized near the nucleus (Fig. 3J, K). Together, these results indicate that Spatial is expressed in a highly specific pattern in germ cells at different stages of spermatogenesis. In addition colocalization studies with β-tubulin indicating Spatial association with the manchette give new insights of Spatial function in morphogenesis.

Distribution of Spatial in isolated germ cells

We further investigated the subcellular localization of Spatial at different stages of spermatid development by confocal microscopy on isolated germ cells (Fig. 4). In most early round spermatids, at the beginning of mouse spermiogenesis, Spatial staining corresponds to vesicle-like profiles distributed all over the cytosol (Fig. 4A). At later stages of round spermatids, a major pool of Spatial migrates towards a side of the cell that could correspond to the region near the newly forming flagellum (Fig. 4B). We confirmed this hypothesis by co-staining with the marker of the Golgi apparatus GM130/Golgin95 (Fig. 4E-G). It is known that in early round spermatids, the Golgi apparatus exists in the acrosome side where it plays a role in exporting vesicles to this structure [16]. However at the end of this process, the Golgi apparatus starts to migrate toward the opposite pole of the cell near the nascent flagellum [16]. By performing co-staining analysis, we saw that in round spermatids when the Golgi apparatus is located very close to the acrosomal vesicle, Spatial has a cytosolic distribution (Fig. 4E). At later stages of round spermatid differentiation when the Golgi apparatus migrates to the opposite pole near the nascent flagellum, Spatial is concentrated in the same area with a partial colocalization (Fig. 4F). At later stages of spermatogenesis during the elongation process, in contrast to the Golgi apparatus which persists in the residual cytoplasm, Spatial is localized to the vicinity of the manchette (Fig. 4C, G). The association of Spatial with the manchette was also confirmed on isolated spermatid cells by co-staining with β- and α-tubulins displaying the same distribution over this structure (Fig. 4H, I). Finally in the spermatozoa, Spatial is specifically associated with the principal piece of the tail (Fig. 4D). Altogether, these results suggest that Spatial distribution correlates with the shaping of the nucleus and the formation of the flagellum during the elongation process of spermatids.

Spatial expression persists in mature spermatozoa

Spermatozoa from the testis showed a well-defined localization of Spatial on the principal piece of the sperm tail (Fig. 4D). To test if Spatial still persists in the tail of mature spermatozoa, sperm was collected from isolated cauda epididymides and vas deferens, then fixed, permeated, and subjected to immunofluorescence (Fig. 5). Sperm of both regions exhibit bright, intense fluorescence over the principal piece of the tail while no fluorescence is observed over the midpiece (Fig. 5A, B). Essentially, no staining was observed in sperm exposed to pre-immune serum instead of primary antibody (Fig. 5C). Results show that Spatial still persists in mature sperm and its expression is limited to a specific compartment of the spermatozoa flagellum.

Association of Spatial with KIF17b in the manchette and the spermatozoa tail

Several studies have identified that Spatial is expressed by highly polarized cell types as stromal cells in the thymus, neurons in the brain in addition to postmeiotic germ cells in the testis [7, 9]. In addition to its distribution all over the principal piece of spermatozoa tail, our laboratory showed that Spatial is also expressed in dendrite extensions restricted to particular neuronal cell types of the central nervous system (unpublished observations). Dendrite and flagellum share similar molecular motor components which are proposed to mobilize cargo proteins along microtubules [17, 18]. Moreover, experiments showed that Spatial colocalizes with a neuron-specific molecular motor KIF17 in dendrites. This molecular motor KIF17 presents a specific testis isoform, KIF17b which is expressed in mature sperm, and mainly localized in the principal piece of the sperm tail [14]. In order to determine if colocalization between Spatial and KIF17 is also conserved in the principal piece of sperm tail, co-staining analysis was performed on testis purified sperm using a polyclonal anti-KIF17 antibody with the affinity-purified anti-Spatial antibody (Fig. 6A-D). The result showed punctuate patterns of colocalization throughout the

principal piece of the spermatozoa tail (Fig. 6A, C). At higher magnification, many punctuate particles of the labelled Spatial (*red*) colocalize with KIF17b (*green*; Fig. 6B inset, D). Particles containing Spatial and KIF17b alone were also detected (Fig. 6B inset, D). In mature sperm purified from the epididymis, Spatial-KIF17b colocalization still persists in the principal piece of the tail (data not shown).

Since preliminary discussions proposed that KIF17b is also associated with the manchette [19] and other data indicated that some of the kinesins are involved in intramanchette transport (IMT) [20, 21], we decided to study Spatial-KIF17b association in this structure (Fig. 6E, F). Co-staining analysis was performed showing punctuate patterns of colocalization all over the manchette (Fig. 6E). Altogether, these results show that Spatial and KIF17 colocalize in highly organized cytoskeletal structures: the manchette and the principal piece of the sperm tail.

To determine whether KIF17b associates with Spatial, we performed co-immunoprecipitation experiments using lysate from homogenized mouse testis (Fig. 7). Because Spatial long isoforms migrate closely with IgG heavy chains, we used resin immobilized antibodies. Precipitated proteins were separated on an SDS-PAGE gel, transferred to filter, and visualized by Western blotting (Fig. 7). Results showed that anti-Spatial antibody efficiently immunoprecipitates both Spatial long isoforms Spatial-ε and -δ as expected (Fig. 7A, left panel). However, rabbit IgG does not pull down these proteins. Interestingly, the Western blot probed with KIF17 antibody demonstrated that KIF17b is also specifically co-immunoprecipitated indicating that Spatial and KIF17b could be a part of a complex *in vivo* (Fig. 7A, right panel). To further explore the interaction between these proteins and determine whether there is any isoform specificity of Spatial in KIF17b interaction, coimmunoprecipitation of native proteins from testis extract was performed with KIF17 antibody (Fig. 7B, left panel). The result showed that KIF17 antibody

efficiently immunoprecipitates Spatial-ε through KIF17b while Spatial-δ is not immunoprecipitated (Fig. 7B, right panel). Then, the association of the kinesin KIF17b with Spatial occurs through Spatial-ε potentially required for their colocalization in the manchette and the principal piece of sperm tail.

DISCUSSION

Spatial was initially identified in the mouse thymus, highly expressed in the subcapsular region constituted of polarized epithelial cells [6, 7]. Analysis of a wide panel of mouse tissues showed that Spatial is also expressed in the testis and the central nervous system [9]. The function of Spatial in these three distinct organs remains completely unknown. This gene generates at least five alternative spliced variants: three short isoforms (Spatial-α, -β and -γ) and two long isoforms (Spatial-ε and -δ) with a tissue specific distribution. In the adult mouse testis, the expression of Spatial is developmentally regulated since it appears from 8 weeks [9]. Spatial mRNA expression is mainly restricted to haploid round spermatids since it corresponds to step 2-10 spermatids. In this article, we characterize the mouse testicular Spatial proteins corresponding to the long isoforms Spatial-ε and Spatial-δ and we show that the short isoform Spatial-β is also expressed in the mouse testis .

Spatial-β protein is specifically expressed in round spermatids to drastically reduce at later stages of spermiogenesis. This diminution could be in correlation with the transcriptional complex ACT/CREM since Spatial-β significantly increases in *act* null mice (supplementary data). ACT is a LIM-only protein playing a crucial role during round spermatid stages in activating the transcription factor CREM that regulates expression of many crucial genes required for spermatid maturation [10, 22, 23]. Since ACT is a trancriptional coactivator, its effect on

Spatial-β downregulation could be indirect by inducing the transcription of some genes required for the downregulation of Spatial-β expression. On the other hand, it could also be possible that ACT is involved in negative regulation of gene expression since the function of ACT as an coactivator is still not defined on specific haploid genes. Consequently, these preliminary results will lead us to evaluate if the transcriptional complex CREM/ACT directly or indirectly regulates the expression of Spatial-β. To investigate this hypothesis, further studies have to be focused on gel shift assays on the Spatial promoter.

Previous work showed that Spatial messengers present the highest signal restricted to step 5-7 round spermatids [9]. The protein expression profile indicates an important amount of the Spatial proteins at step 7-9 spermatids which correspond to the beginning of spermatid elongation and the flagellum biogenesis [2]. We further examined by confocal microscopy the cellular distribution of Spatial on isolated germ cells during this process. We found that Spatial presents a vesicle-like distribution all over the cytosol in early round spermatids and is subsequently concentrated in the opposite pole of the acrosome near the newly nascent flagellum at later stages of round spermatids. First, we investigated the vesicle-like distribution of Spatial in early round spermatids. Indeed, it is known that vesicular trafficking during early spermiogenesis seems to be unique since it is associated with the shaping and the remodelling of the acrosome [16]. We performed co-staining with markers of vesicles involved in the development and the shaping of the acrosome as Clathrin located in the trans-Golgi of early round spermatids and lysosomal proteins, LAMP-1 and LAMP-2, distributed through the cytosol [16, 24]. No colocalization was obtained with Spatial proteins (data not shown). All these results strongly suggest that Spatial does not exist in the vesiclar network involved in acrosome formation. However, Spatial partially colocalizes with the GM130/Golgin95 a marker of the Golgi apparatus that also migrates toward

the region of the nascent flagellum after the formation of the acrosome [16]. At later stages, when the Golgi apparatus appears in the residual cytoplasm, Spatial is associated with the manchette which is known to manage the elongation of spermatids head and the formation of the sperm tail [5, 25]. By considering the cellular distribution of Spatial, we can propose that it is related to morphogenesis which leads to the elongation of round spermatids and the formation of the sperm tail.

This hypothesis does not exclude the possibility that Spatial could also be part of the structural protein family that participates in the architectural organization of the flagellum, since it persists in the principal piece of the mature epididymal and vas deferens sperm. No staining was revealed in the end piece of the flagellum with no accessory structures and in the midpiece presenting the mitochondrial sheath [26]. The principal piece is composed of a unique cytoskeletal structure called the fibrous sheath surrounding the axoneme [27]. Recent studies have revealed the molecular structures and functions of a number of axonemal and fibrous sheath components, including motor molecules, structural proteins, receptors and channels involved in different functions such as sperm maturation, motility, capacitation, hyperactivation and glycolysis [28]. At this stage, additional experiments are needed to find out in which structure or pathway of the principal piece Spatial exists in order to understand its function.

For cellular morphogenesis, intracellular transport is fundamental, since complex macromolecular structures (e.g., flagella, cilia, neurite) and polarized specializations need means to deliver and localize molecules. The kinesin superfamily proteins KIFs participate in this selective transport by using adaptator or scaffolding proteins that recognize and bind cargoes such as membranous organelles, protein complexes, channels and mRNAs [29-33]. In neurons, it is becoming clear how cargoes are directed to axons and dendrites by KIFs, while in the testis their involvement in mammalian intramanchette and intraflagellar transports has not yet been

well studied [18, 34-37]. As indicated, Spatial is expressed in dendrite extensions restricted to particular neuronal cell types of the mouse adult brain (unpublished observations). Interestingly in these particular neuronal cell types, two kinesin motors KIF5 and KIF17 were well defined to be involved in the dendritic transport [18, 34, 36, 37]. In the testis, isoforms of these two kinesin motors were characterized: (1) KIF5a and KIF5b which are expressed during meiosis [38], (2) KIF5c weakly expressed in spermatids and not detectable in sperm tail [38], and (3) KIF17b expressed all over spermatogenesis to persist in sperm tail [10, 14].

In the testis, KIF17b seems to have two mechanisms of mobilization. (1) One of them constitutes a phosphorylation of KIF17b by the protein kinase A to shuttle between the nuclear and cytoplamic compartments [19]. This mechanism controls the transport of the CREM coactivator molecule ACT in round spermatids [10, 19]. (2) In elongating spermatids and mature sperm, it was proposed that the mechanism of mobilization might switch to the more traditional microtubule-dependant mode at a time when KIF17b is associated with the manchette [5] and the principal piece of the sperm tail [14]. Cargoes associated with KIF17b during these later stages of spermatogenesis have not as yet been identified. By confocal analysis and immunoprecipitation experiments of native proteins, we showed that Spatial is associated with KIF17b in the manchette of elongating spermatids and in the principal piece of the spermatozoa tail and could thus be one of its cargoes in these highly organized cytoskeletal structures.

Although, the precise function of kinesin subunits in the mouse spermatid manchette and flagellum is unknown, it is suggested to be involved in mediating intramanchette transport (IMT) and intraflagellar transport (IFT) [20]. It is to be assumed that a molecular and functional correlation exist between IFT and IMT. It is due by the fact that molecular motors are present in the manchette with an increasing number of structural and functional proteins initially housed in the manchette before relocating to the centrosome and the developing tail [20, 25]. Interestingly,

Spatial-KIF17b colocalization was first identified all over the manchette to finally persist in the principal piece of the sperm tail with punctuate and discontinuous staining as the distribution obtained with other kinesins [38-40]. Furthermore, KIF17b was co-immunoprecipitated with Spatial long isoforms and more specifically this molecular motor is associated with the isoform Spatial-ε. It has to be noted that Spatial long isoforms contains a carboxy-terminal motif (RVHP; amino acids 291-294 for Spatial-ε and amino acids 257-260 for Spatial-δ). It was shown that the RVxP motif is implicated in the ciliary localization of membrane proteins [31, 41]. One of these proteins is CNGB1b, a subunit of the cyclic nucleotide-gated (CNG) channels associated with the kinesin KIF17 in olfactory sensory neurons [31]. It was shown that both the RVxP motif of CNGB1b and KIF17 association are required for ciliary targeting of these protein channels [31]. Additional experiments based on (1) amino acids substitutions of this motif and (2) KIF17 inhibition need to be perform in order to demonstrate the requirements of these factors for Spatial extension targeting. Then, in mouse neurons it was clearly shown that ciliary and dendritic targeting requires the kinesin-2 motor, KIF17 [31, 36, 37]. However, the role for KIF17 isoform in cytoskeletal structures of mouse testis has never been described. Whether KIF17 evolved distinct roles in cilia, dendrite and flagellum or can execute a similar function in these structures remain an open question. Further work will be necessary to understand the cellular mechanism to which Spatial-KIF17b assembly is associated in order to find Spatial function during spermatogenesis.

In summary, this work provides evidence for the presence of Spatial-β with a specific function in round spermatids and the contribution of Spatial long isoforms in spermatid morphogenesis. In addition, There is growing evidence pointing to Spatial-KIF17 association through Spatial-ε in the manchette and the flagellum. Finally, evidence is presented consistent

with the contribution of each isoform in specific functions through different organs where Spatial seems to be involved in developmental process.

Acknowledgements

We thank Dr. Eddy Mitch (NIH, North Carolina, USA), Dr. Lee Leserman (CIML, Marseille France) and Dr. Philippe Benech (TAGC, Marseille, France) for their helpful comments on the manuscript. This work was supported by the Institut National de la Santé et de la Recherche Médicale (INSERM). Murielle Saade is supported by a grant from the INSERM/Provence-Alpes-Côte d'Azur region and Magali Irla was supported by a PhD fellowship from the Association pour la Recherche sur le Cancer (ARC).

References

[1] E. F. Oakberg, A description of spermiogenesis in the mouse and its use in analysis of the cycle of the seminiferous epithelium and germ cell renewal. Am J Anat 99 (1956) 391-413.

[2] A. L. Kierszenbaum, and L. L. Tres, Structural and transcriptional features of the mouse spermatid genome. J Cell Biol 65 (1975) 258-70.

[3] A. Akhmanova, A. L. Mausset-Bonnefont, W. van Cappellen, N. Keijzer, C. C. Hoogenraad, T. Stepanova, K. Drabek, J. van der Wees, M. Mommaas, J. Onderwater, H. van der Meulen, M. E. Tanenbaum, R. H. Medema, J. Hoogerbrugge, J. Vreeburg, E. J. Uringa, J. A. Grootegoed, F. Grosveld, and N. Galjart, The microtubule plus-end-tracking protein CLIP-170 associates with the spermatid manchette and is essential for spermatogenesis. Genes Dev 19 (2005) 2501-15.

[4] M. L. Meistrich, B. O. Reid, and W. J. Barcellona, Changes sperm culei during sperimogensis and epidymal maturation. Exp Cell Res 99 (1976) 72-8.

[5] A. L. Kierszenbaum, and L. L. Tres, The acrosome-acroplaxome-manchette complex and the shaping of the spermatid head. Arch Histol Cytol 67 (2004) 271-84.

[6] A. Carrier, C. Nguyen, G. Victorero, S. Granjeaud, D. Rocha, K.Bernard, A. Miazek, P. Ferrier, M. Malissen, P. Naquet, B. Malissen, and B. R. Jordan, Differential gene expression in CD3epsilon- and RAG1-deficient thymuses: definition of a set of genes potentially involved in thymocyte maturation. Immunogenetics 50 (1999) 255-70.

[7] F. A. Flomerfelt, M. G. Kim, and R. H. Schwartz, Spatial, a gene expressed in thymic stromal cells, depends on three-dimensional thymus organization for its expression. Genes Immun 1 (2000) 391-401.

[8] M. Irla, D. Puthier, S. Granjeaud, M. Saade, G. Victorero, M. G. Mattei, and C. Nguyen, Genomic organization and the tissue distribution of alternatively spliced isoforms of the mouse Spatial gene. BMC Genomics 5 (2004) 41.

[9] M. Irla, D. Puthier, R. Le Goffic, G. Victorero, T. Freeman, P. Naquet, M. Samson, and C. Nguyen, Spatial, a new nuclear factor tightly regulated during mouse spermatogenesis. Gene Expr Patterns 3 (2003) 135-8.

[10] B. Macho, S. Brancorsini, G. M. Fimia, M. Setou, N. Hirokawa, and P. Sassone-Corsi, CREM-dependent transcription in male germ cells controlled by a kinesin. Science 298 (2002) 2388-90.

[11] A. R. Bellve, Purification, culture, and fractionation of spermatogenic cells. Methods Enzymol 225 (1993) 84-113.

[12] Y. Marushige, and K. Marushige, Proteolysis of somatic type histones in transforming rat spermatid chromatin. Biochim Biophys Acta 761 (1983) 48-57.

[13] K. J. Livak, and T. D. Schmittgen, Analysis of relative gene expression data using real-time quantitative PCR and the 2(-Delta Delta C(T)) Method. Methods 25 (2001) 402-8.

[14] N. Kotaja, D. De Cesare, B. Macho, L. Monaco, S. Brancorsini, E. Goossens, H. Tournaye, A. Gansmuller, and P. Sassone-Corsi, Abnormal sperm in mice with targeted deletion of the act (activator of cAMP-responsive element modulator in testis) gene. Proc Natl Acad Sci U S A 101 (2004) 10620-5.

[15] F. Nantel, L. Monaco, N. S. Foulkes, D. Masquilier, M. LeMeur, K. Henriksen, A. Dierich, M. Parvinen, and P. Sassone-Corsi, Spermiogenesis deficiency and germ-cell apoptosis in CREM-mutant mice. Nature 380 (1996) 159-62.

[16] R. D. Moreno, J. Ramalho-Santos, P. Sutovsky, E. K. Chan, and G. Schatten, Vesicular traffic and golgi apparatus dynamics during mammalian spermatogenesis: implications for acrosome architecture. Biol Reprod 63 (2000) 89-98.

[17] S. A. Baker, K. Freeman, K. Luby-Phelps, G. J. Pazour, and J. C. Besharse, IFT20 links kinesin II with a mammalian intraflagellar transport complex that is conserved in motile flagella and sensory cilia. J Biol Chem 278 (2003) 34211-8.

[18] N. Hirokawa, and R. Takemura, Molecular motors and mechanisms of directional transport in neurons. Nat Rev Neurosci 6 (2005) 201-14.

[19] N. Kotaja, B. Macho, and P. Sassone-Corsi, Microtubule-independent and protein kinase A-mediated function of kinesin KIF17b controls the intracellular transport of activator of CREM in testis (ACT). J Biol Chem 280 (2005) 31739-45.

[20] A. L. Kierszenbaum, Intramanchette transport (IMT): managing the making of the spermatid head, centrosome, and tail. Mol Reprod Dev 63 (2002) 1-4.

[21] M. G. Miller, D. J. Mulholland, and A. W. Vogl, Rat testis motor proteins associated with spermatid translocation (dynein) and spermatid flagella (kinesin-II). Biol Reprod 60 (1999) 1047-56.

[22] G. M. Fimia, D. De Cesare, and P. Sassone-Corsi, CBP-independent activation of CREM and CREB by the LIM-only protein ACT. Nature 398, (1999). 165-9.

[23] G. M. Fimia, D. De Cesare, and P. Sassone-Corsi, A family of LIM-only transcriptional coactivators: tissue-specific expression and selective activation of CREB and CREM. Mol Cell Biol 20 (2000) 8613-22.

[24] R. D. Moreno, Differential expression of lysosomal associated membrane protein (LAMP-1) during mammalian spermiogenesis. Mol Reprod Dev 66 (2003) 202-9.

[25] A. L. Kierszenbaum, Spermatid manchette: plugging proteins to zero into the sperm tail. Mol Reprod Dev 59 (2001) 347-9.

[26] E.M. Eddy, D.A. O'Brian, The Spermatozoon. In: Knobil, Neill JD (eds.), The Physiology of Reproduction, vol. 2. New York: Raven Press; (1994) 29-77.
[27] D. W. Fawcett, The mammalian spermatozoon. Dev Biol 44 (1975) 394-436.
[28] K. Inaba, Molecular architecture of the sperm flagella: molecules for motility and signaling. Zoolog Sci 20 (2003) 1043-56.
[29] R. D. Vale, The molecular motor toolbox for intracellular transport. Cell 112 (2003) 467-80.
[30] V. Chennathukuzhi, C. R. Morales, M. El-Alfy, and N. B. Hecht, The kinesin KIF17b and RNA-binding protein TB-RBP transport specific cAMP-responsive element modulator-regulated mRNAs in male germ cells. Proc Natl Acad Sci U S A 100 (2003) 15566-71.
[31] P. M. Jenkins, T. W. Hurd, L. Zhang, D. P. McEwen, R. L. Brown, B. Margolis, K. J. Verhey, and J. R. Martens, Ciliary targeting of olfactory CNG channels requires the CNGB1b subunit and the kinesin-2 motor protein, KIF17. Curr Biol 16 (2006) 1211-6.
[32] P. J. Chu, J. F. Rivera, and D. B. Arnold, A role for Kif17 in transport of Kv4.2. J Biol Chem 281 (2006) 365-73.
[33] N. Kotaja, H. Lin, M. Parvinen, and P Sassone-Corsi, Interplay of PIWI/Argonaute protein MIWI and kinesin KIF17b in chromatoid bodies of male germ cells. J Cell Sci 119 (2006) 2819-25.
[34] N. Hirokawa, and R. Takemura, Kinesin superfamily proteins and their various functions and dynamics. Exp Cell Res 301 (2004) 50-9.
[35] J. L. Rosenbaum, and G. B. Witman, Intraflagellar transport. Nat Rev Mol Cell Biol 3 (2002) 813-25.
[36] L. Guillaud, M. Setou, and N. Hirokawa, KIF17 dynamics and regulation of NR2B trafficking in hippocampal neurons. J Neurosci 23(2003) 131-40.
[37] M. Setou, T. Nakagawa, D. H. Seog, and N. Hirokawa, Kinesin superfamily motor protein KIF17 and mLin-10 in NMDA receptor-containing vesicle transport. Science 288 (2000) 1796-802.
[38] A. Junco, B. Bhullar, H. A. Tarnasky, and F. A. van der Hoorn, Kinesin light-chain KLC3 expression in testis is restricted to spermatids. Biol Reprod 64 (2001) 1320-30.
[39] M. Ihara, A. Kinoshita, S. Yamada, H. Tanaka, A. Tanigaki, A. Kitano, M. Goto, K. Okubo, H. Nishiyama, O. Ogawa, C. Takahashi, S. Itohara, Y. Nishimune, M. Noda, and M. Kinoshita, Cortical organization by the septin cytoskeleton is essential for structural and mechanical integrity of mammalian spermatozoa. Dev Cell 8 (2005) 343-52.
[40] J. H. Henson, D. G. Cole, C. D. Roesener, S. Capuano, R. J. Mendola, and J. M. Scholey, The heterotrimeric motor protein kinesin-II localizes to the midpiece and flagellum of sea urchin and sand dollar sperm. Cell Motil Cytoskeleton 38 (1997) 29-37.
[41] L. Geng, D. Okuhara, Z. Yu, X. Tian, Y. Cai, S. Shibazaki, and S. Somlo, Polycystin-2 traffics to cilia independently of polycystin-1 by using an N-terminal RVxP motif. J Cell Sci 119 (2006) 1383-95.

LEGENDS

Fig. 1- Characterization of Spatial (Sp) protein isoforms in mouse round spermatids. A purified polyclonal anti-Spatial antibody was generated in rabbits. (A) Western blot analysis on proteins extracted from a pool of round spermatids (RS) separated into non-soluble (ns) and soluble (s) extracts was peformed to study the specificity of this antibody. The result shows three intense bands in the cytosoluble fraction at 52, 49 and 34 kDa corresponding to Spatial-ε, Spatial-δ and Spatial-β, respectively. β-tubulin was used as a loading control for protein concentration. Position of the protein molecular weight marker is seen to the left. (B) Quantitative TaqMan RT-PCR analysis was performed, using primers specific for short isoforms (reflecting the Spatial-β expression) on purified pachytene spermatocytes (PS), round spermatids (RS) and a pool of round-elongating spermatids (RES). For this experiment, the highest expression level was considered as 1.

Fig. 2- Expression of Spatial isoforms during spermatogenesis. (A) Western blot analysis was performed on mouse isolated germ cell types. PS: pachytene spermatocytes, RS: round spermatids, RES: round and elongating spermatids, ES: elongated spermatids, CS: condensed spermatids and Spz: spermatozoa. β-tubulin was used as loading control for protein concentration. The transition protein 2 (TP2) expression was used as criteria of fractionation quality. (B) Quantitative analysis of the blot using image J software shows a high expression of long Spatial proteins during the elongation of spermatids (RES-ES) to further decrease in condensed spermatids (CS) and to persist in spermatozoa (Spz) while Spatial-β short isoform is exclusively highly expressed in round spermatids (RS). Three different experiments were performed for the quantification analysis, $n = 3$.

Fig. 3- Localization of Spatial in the adult mouse testis. (A-C, E-G) Immunofluorescence staining of 10 week-old mouse testis cryosections was performed using the affinity-purified anti-Spatial antibody (*red*). Cell nucleus is identified by DAPI counterstaining. Views show different spermatogenic stages corresponding to distinct tubules: (A,B) the brightest fluorescence correspond to round spermatids at stage VIII of seminiferous tubules differentiation and elongating spermatids at stages IX-X. (C) A staining of the developing sperm tails is shown in seminiferous tubules at stages XI-XII. (E-G) In tubules where round and elongating spermatids exist respectively, bright fluorescence occurs over structures or organelles near the nucleus of some round spermatids (arrowheads, E) to correspond to a ring-like staining surrounding the head region of elongating spermatids (arrowheads F, G). (D) No staining was observed in testis cryosections exposed to pre-immune serum in place of primary antibody. (H, K) Testis sections of mice were also subjected to immunohistochemistry. Hematoxylin was used for counterstaining. Both views H and I show the distribution of Spatial in seminiferous tubules in spermatogenic stages VIII and IX–X, respectively. (J) A higher magnification of seminiferous tubules at stages VII-VIII shows a cytosolic distribution of Spatial in early round spermatids. (K) A punctuate staining also occurred over structures near the spermatid nucleus at stages VIII-IX represented by arrowheads. (Inset I) In elongating spermatids, Spatial appears to be associated with the manchette represented by arrows. (L-N) The manchette distribution of Spatial was strengthened by colocalization studies with β-tubulin on testis cryosections. (A-D, H, I, L-N) Scale bar = 50 µm, (E-G, J, K) scale bar = 5 µm.

Fig. 4- Analysis of Spatial subcellular distribution in isolated mouse germ cells. (A-I) Germ cells isolated from mouse testis were permeabilized and analysed by immunofluorescence. (A) In early

round spermatids, Spatial (*red*) presents a cytosolic distribution. (B) At later stages of round spermatids Spatial is concentrated in the opposite phase of the acrosome near the nascent flagellum. (C) In elongating spermatids Spatial distribution appears to be associated with the manchette. (D) In the spermatozoa Spatial persists in the principal piece of the tail. Arrow indicates location of the midpiece. Cells were identified by phase contrast observation (insets) and nuclei were stained with DAPI (*blue*). (E-G) Spermatids were also subjected to immunofluorescence analysis of Spatial (*red*) distribution versus the Golgi protein Golgin-95 (*green*) with the DAPI counterstaining (*blue*) and identification by phase contrast observation (insets). (E) In early round spermatid the Golgi apparatus is facing the acrosome while Spatial has a cytosolic distribution. (F) At later stages of round spermatid differentiation the Golgi apparatus migrates towards the opposite pole of the cell near the nascent flagellum where Spatial is also concentrated. This result confirm that the polarized staining of Spatial in B corresponds to the region near the nascent flagellum. (G) In elongating spermatids Spatial distribution appears to be associated with the manchette while the Golgi apparatus appears in the residual cytoplasm. (Inset G) Arrows indicate location of the manchette consisting of a thin black structure surrounding the nucleus. (H, I) The manchette distribution of Spatial was also confirmed by colocalization studies with β- and α-tubulins (*green*) on purified elongating spermatids. (A-C, E-I) Scale bar = 5 µm; (D) scale bar= 3 µm.

Fig. 5- Analysis of Spatial distribution in maturing spermatozoa. (A, B) Phase contrast images (right) and immunofluorescent localization (left) of Spatial with the cell nuclear DAPI counterstaining (*blue*) in isolated mice cauda epididymal and vas deferens sperm, respectively. Arrows indicate location of the midpiece in representative sperm. In the sperm of these two areas,

Spatial localizes exclusively to the principal piece of the sperm tail. (C) No staining was observed in sperm exposed to pre-immune serum in place of primary antibody. Scale bar = 8 μm.

Fig. 6- Spatial and KIF17b colocalize in highly organized structures. (A-D) Spermatozoa in dissociated culture from seminiferous tubules are stained for endogenous Spatial (*red*) and for KIF17b (*green*). (A, C) Regions inside the blue box on the low power images corresponding to the principal piece of the spermatozoa tail are shown in high power images in B and D. (Inset B, D) Small arrows point the colocalization of Spatial and KIF17b (*yellow*) in the principal piece of the spermatozoa tail. (A-D) The position of the unstained midpiece of the spermatozoa tail is oriented by the arrow, pointing toward the nucleus. (E, F) Elongating spermatids in dissociated culture from seminiferous tubules were stained for endogenous Spatial (*red*) and for KIF17b (*green*) showing colocalization (*yellow*) in the manchette. (A, C) Scale bar = 20 μm, (B, D, E, F) scale bar = 5 μm, (inset B) scale bar = 1 μm.

Fig. 7- Association of native Spatial and KIF17b proteins. (A, left panel) The complex precipitated from testis lysate with the resin immobilized Spatial antibody contains both Sp-ε and Sp-δ proteins as assessed by immunoblotting (IB) with anti-Spatial antibody. (Right panel) Endogenous KIF17b co-immunoprecipitates (IP) with Spatial from testis lysate. as assessed by immunoblotting with anti-KIF17 antibody. (B) A reverse co-immunoprecipitation with endogenous KIF17b shows its association with Spatial through Sp-ε as assessed by IB with anti-KIF17 and anti-Spatial antibodies, respectively. In contrast, rabbit IgG did not pull down these proteins. Molecular weight markers (in kDa) are shown to the left of the blots.

Supplemental Fig. 2- Analysis of Spatial expression in the testis of *act* null mice. (A) Quantitative TaqMan RT-PCR was performed to evaluate the expression of Spatial isoforms in the testis of *act* null mice (*act* $^{-/-}$). The expression level of Spatial in the *wild-type* phenotype (*act* $^{+/+}$) was considered as 1. The result shows an increase of Spatial-β isoform while the expression of Spatial long isoforms displays little or no modification in the absence of ACT. (B) The overexpression of Spatial-β in the absence of ACT is also confirmed by Western blot analysis. β-tubulin was used as loading control for protein concentration.

Figure

A

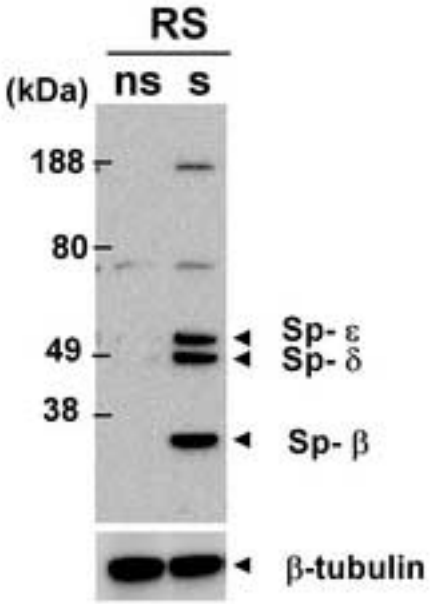

B

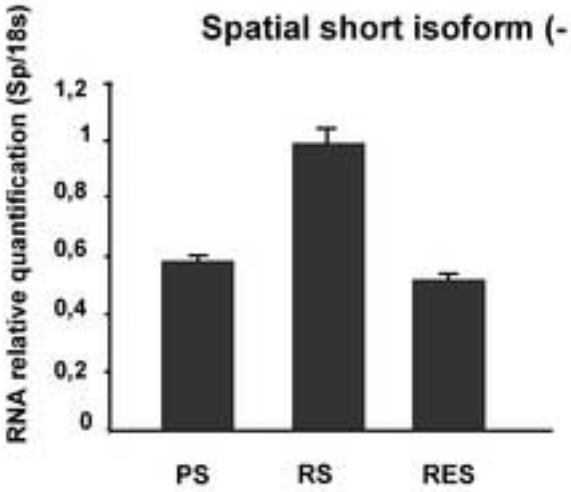

Figure

ck here to download high resolution image

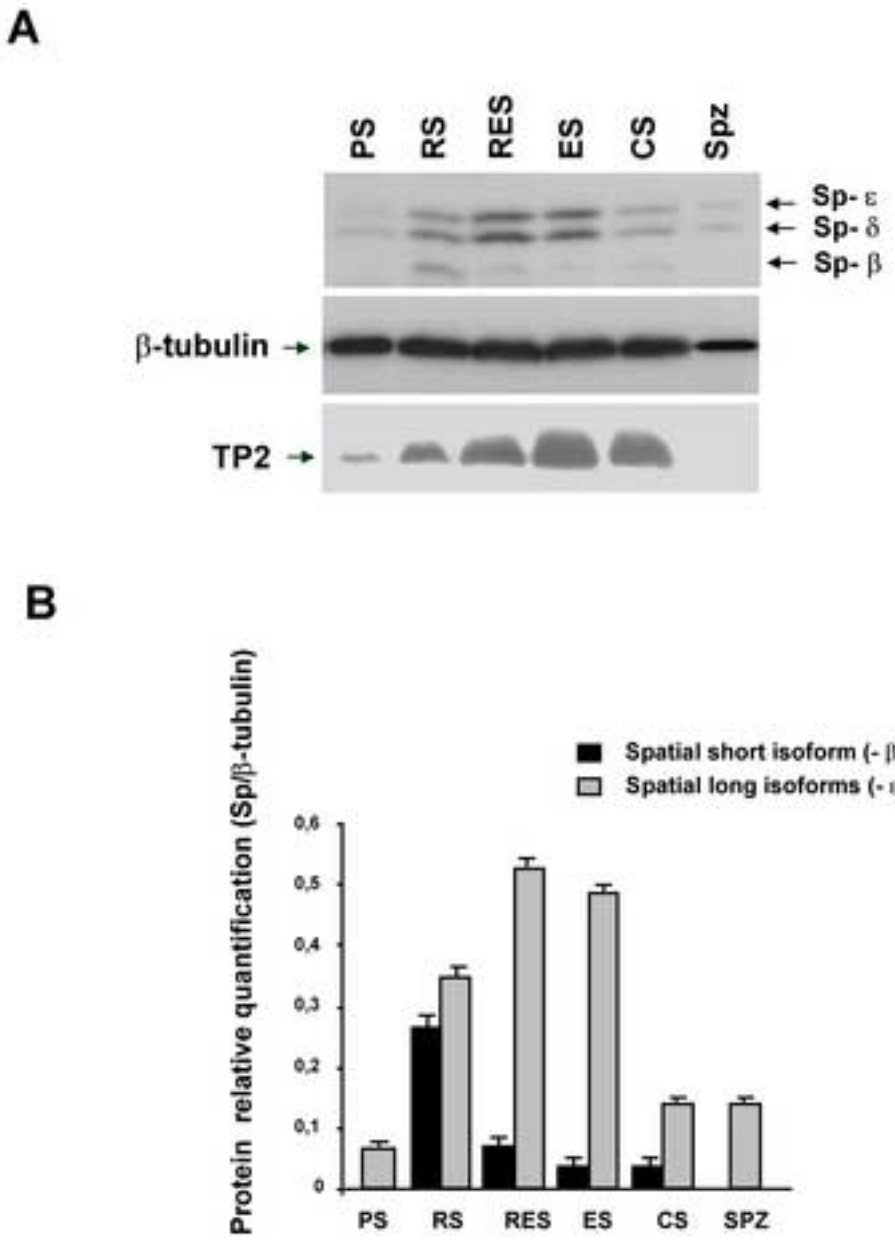

Figure

ck here to download high resolution image

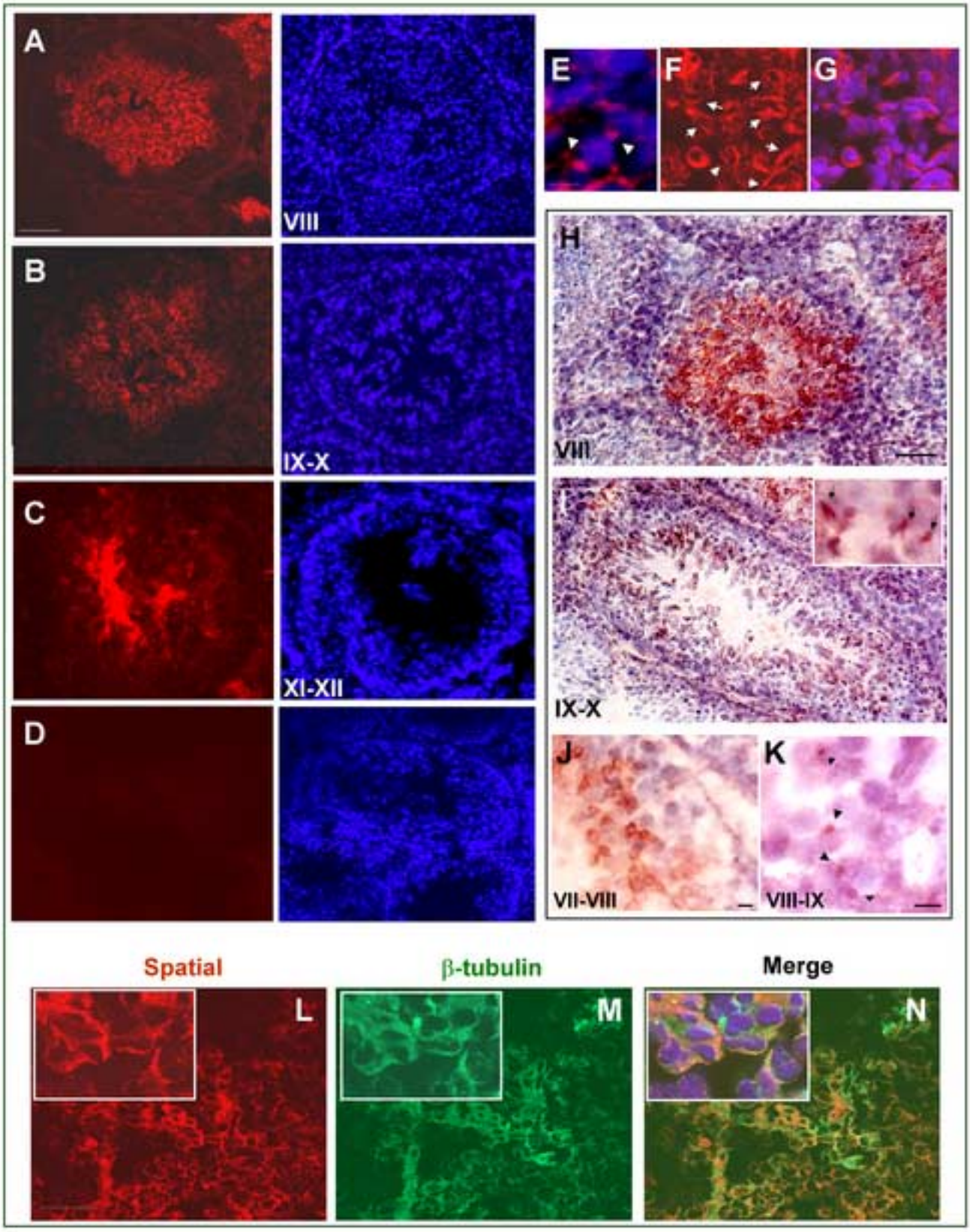

Figure

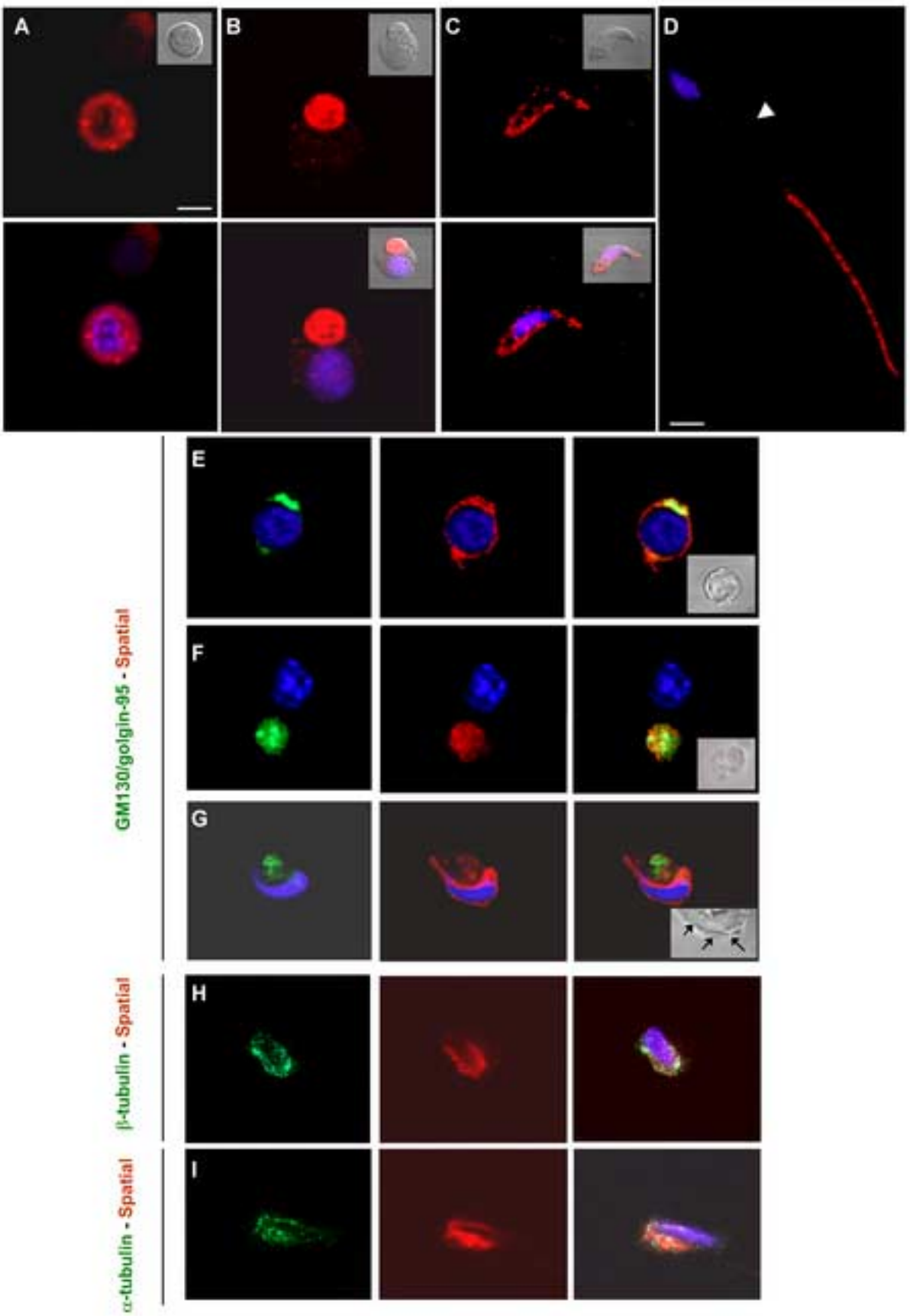

Figure

ck here to download high resolution image

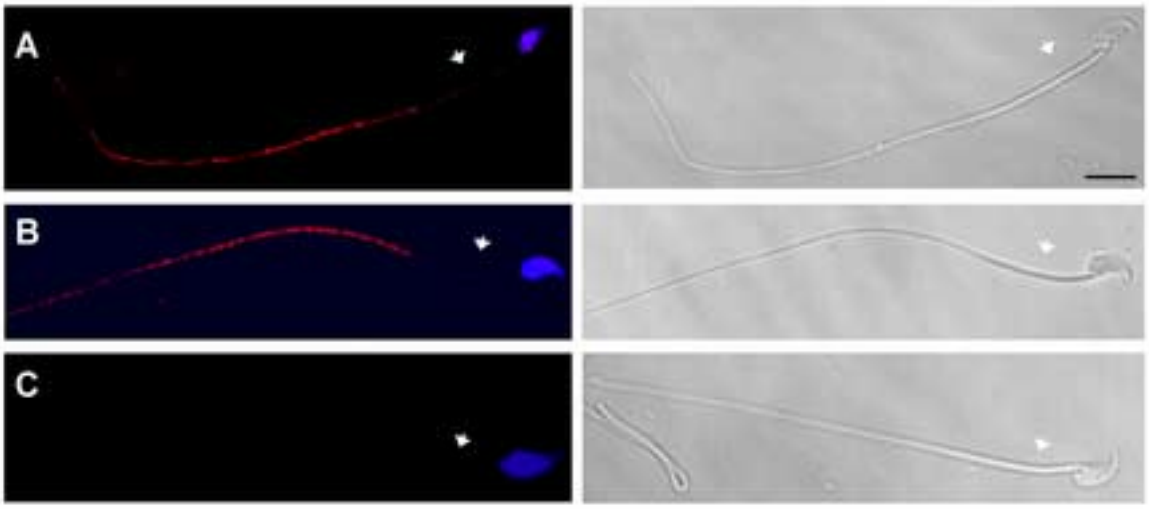

Figure

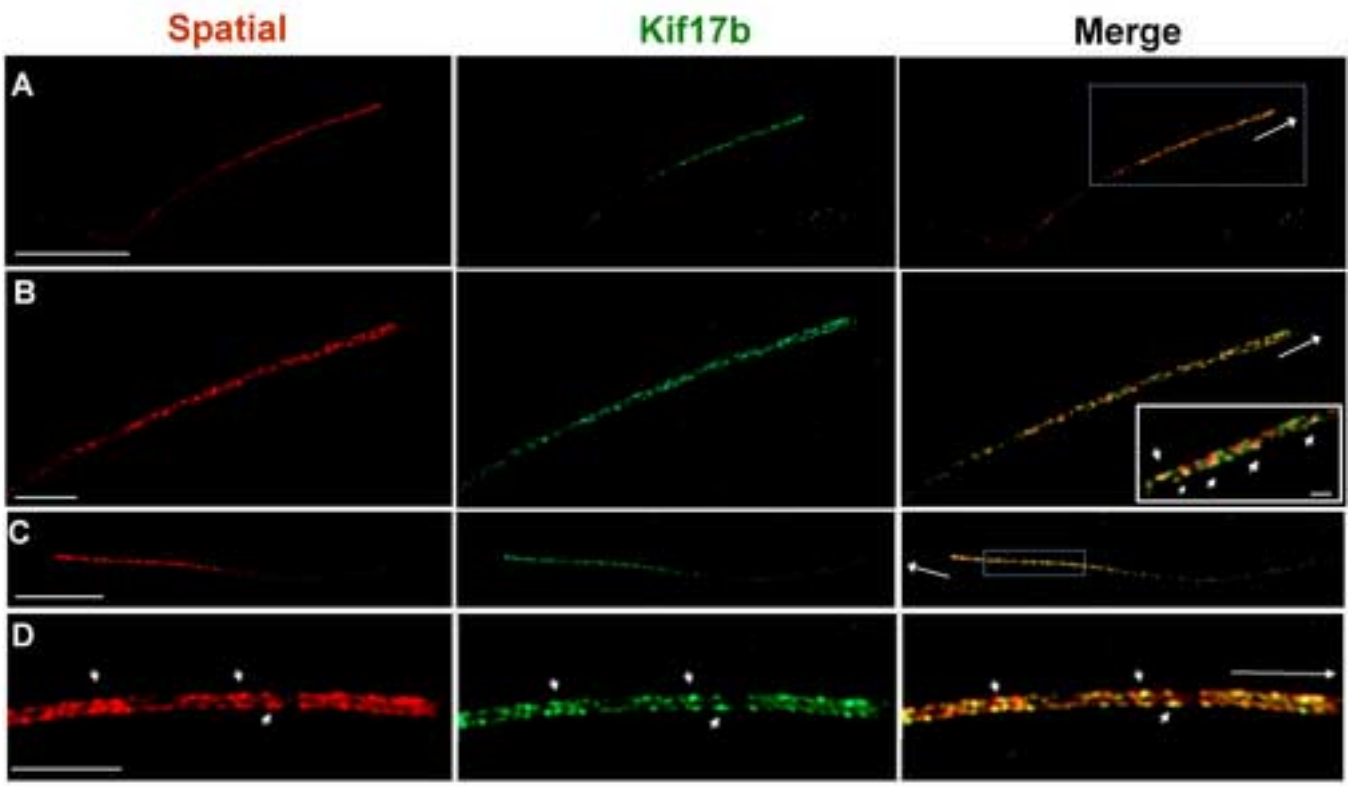

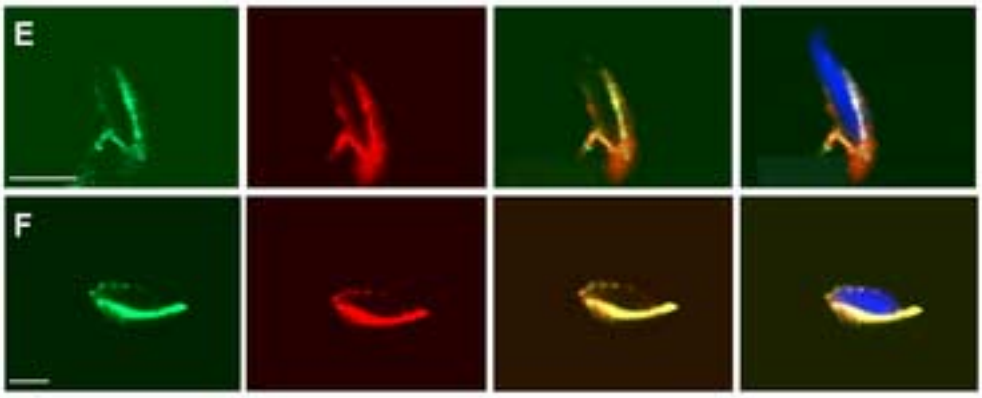

Figure